THE JOURNAL OF PHYSICAL CHEMISTRY Letters

Letter

pubs.acs.org/JPCL

# An Analytical Solution for Exciton Generation, Reaction, and Diffusion in Nanotube and Nanowire-Based Solar Cells

Darin O. Bellisario,[‡] Joel A. Paulson,[†] Richard D. Braatz,[†] and Michael S. Strano*[,†]

[†]Department of Chemical Engineering, Massachusetts Institute of Technology, Cambridge, Massachusetts 02139, United States
[‡]Department of Chemistry, Massachusetts Institute of Technology, Cambridge, Massachusetts 02139, United States

Supporting Information

**ABSTRACT:** Excitonic solar cells based on aligned or unaligned networks of nanotubes or nanowires offer advantages with respect of optical absorption, and control of excition and electrical carrier transport; however, there is a lack of predictive models of the optimal orientation and packing density of such devices to maximize efficiency. Here-in, we develop a concise analytical framework that describes the orientation and density trade-off on exciton collection computed from a deterministic model of a carbon nanotube (CNT) photovoltaic device under steady-state operation that incorporates single- and aggregate-nanotube photophysics published earlier (Energy Environ Sci, 2014, 7, 3769). We show that the maximal film efficiency is determined by a parameter grouping, $\alpha$, representing the product of the network density and the effective exciton diffusion length, reflecting a cooperativity between the rate of exciton generation and the rate of exciton transport. This allows for a simple, master plot of EQE versus film thickness, parametric in $\alpha$ allowing for optimal design. This analysis extends to any excitonic solar cell with anisotropic transport elements, including polymer, nanowire, quantum dot, and nanocarbon photovoltaics.

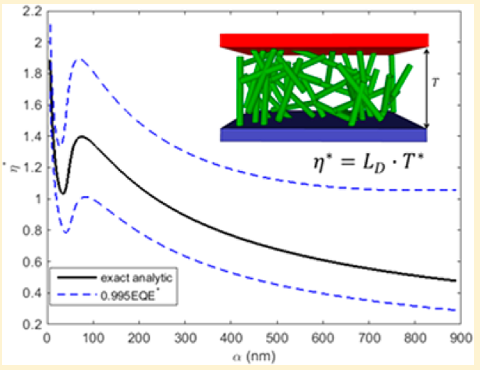


Nanostructured photovoltaics (PVs), e.g., dye-sensitized solar cells (DSSCs), organic PVs, nanoporous metal oxide, and single-walled carbon nanotube (SWCNT) solar cells, have unique advantages for solar energy with respect to cost, efficiency, morphology, and spectral coverage.[1,2] In contrast to bulk-semiconductor solar cells, materials with nanometer scale heterogeneity remain challenging for mathematical modeling.[3−6] For example, the interaction lengths can be too long for *ab initio* treatment but too short for bulk, averaged properties. This heterogeneity often generates an empirically intractable parameter space. Accordingly, it is not obvious how to improve the efficiency of recent carbon nanotube photovoltaic devices.[7−9] In recent work, we developed a physics based approach to modeling exciton generation, transport, and recombination in a single walled carbon nanotube photovoltaic.[10] The deterministic model considered a steady-state planar-heterojunction device incorporating SWCNT photophysics. We found that there existed an optimal thickness beyond which efficiency decreased rapidly. The system of nonlinear nonhomogenous integro-differential equations, however, required numerical evaluation. In this work, we perform a detailed parametric analysis of the previous deterministic model, and develop an analytical model that describes the optimal thickness of the photovoltaic as a function of nanotube density and photophysical constants. We find that the optimal thickness is approximately the effective exciton diffusion length for a given defect density, nanotube length and intrinsic excition diffusivity.

*Exciton Transport Model.* In our previous work, we considered a monochiral network of single-walled nanotubes (SWCNT) sandwiched between two type-II exciton dissociation electrode semi-infinite plates separated by a distance $T$ (Figure 1).[10] The Cartesian $z$ axis is normal to the plates, with the incident solar photon flux $J_0(\omega)$ normally incident at $z = 0$. A given nanotube in the film has orientation $\hat{\mathbf{l}} \equiv (\theta, \phi)$, where $\theta$ is the angle with the $z$ axis. When the network density is high enough (above the percolation threshold), the film can then be meaningfully described by the distribution $p(\theta, \phi)$, with $p(\theta, \phi) = \delta(\theta - \theta')\delta(\phi)$ for example representing an aligned film at angle $\theta'$.[10]

Exciton diffusion occurs via three channels. Longitudinal transport is along the nanotube length, with diffusion coefficient $D_l$. Exciton energy transfer occurs between neighboring tubes either in bundles or at misaligned interconnects, in both cases being orthogonal to the longitudinal axis of the originating nanotube. Those effective diffusion coefficients are $D_{EET,b}$, dependent on the mean bundle size, and $D_{EET,l}$, respectively. $D_l$ is approximately 5 orders of magnitude larger than the latter two. The net exciton diffusivity in the $z$ axis is then achieved by integrating these effects over the film orientation distribution[10]

**Received:** May 16, 2016
**Accepted:** June 30, 2016
**Published:** June 30, 2016





DOI: 10.1021/acs.jpclett.6b01053
J. Phys. Chem. Lett. 2016, 7, 2683−2688

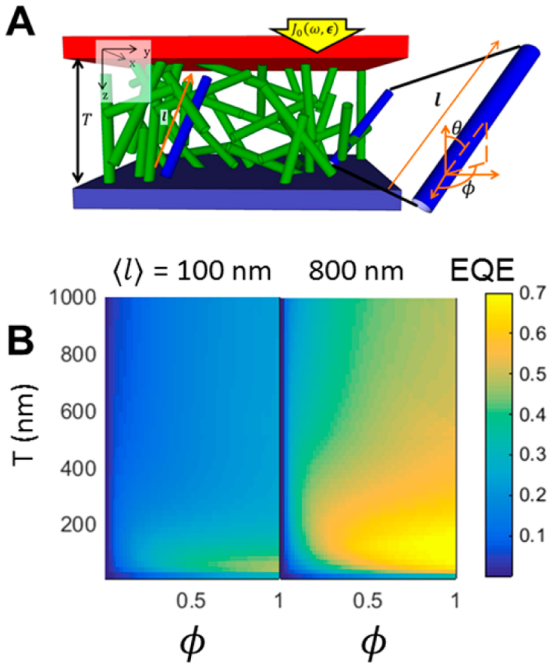


**Figure 1.** (A) Cartoon of a SWCNT solar cell of thickness $T$, with diameters exaggerated. (B) Numerical solution to the steady-state behavior of the vertically aligned film, with the external quantum efficiency (EQE) plotted (colormap) versus the film thickness $T$ and the density $\phi$ as a fraction of the close-packed density, at two different mean nanotube lengths $\langle l \rangle$. Longer tubes exhibit less end-quenching, increasing EQE and allowing the film to be thicker to capture more light while still collecting excitons at the electrodes.

$$D_z \equiv \int\int p(\theta, \phi)[(\cos\theta)^2 D_l + (1 - \cos\theta)^2(\gamma_I D_{EET,I} + b_c D_{EET,b})]\, d\theta\, d\phi \quad (1)$$

where $b_c$ is the bundle fraction in the film (typically near unity) and $\gamma_I$ is a sparsity coefficient capturing the density of interconnects. The exciton population balance can then be constructed by accounting for fluorescent emission, non-radiative decay, Auger recombination, and tube-end quenching,

$$\frac{dc}{dt} = N(z) + D_z\frac{d^2c}{dz^2} - k_\Gamma c - k_1' c - \frac{k_{EEA}}{\rho_{\langle l \rangle}}c^2 - \frac{k_{end}}{\rho_{\langle l \rangle}}\frac{2}{\langle l \rangle}\cdot c \quad (2)$$

where $c(z)$ is the exciton concentration, $N(z)$ is the exciton generation rate from light absorption, $k_{EEA}$ is the auger recombination rate constant, $k_\Gamma$ is the radiative decay rate constant, $k_1'$ is the impurity quenching rate constant proportional to the concentration of impurities, $k_{end}$ is the end-quenching rate constant, and $\langle l \rangle$ is the mean nanotube length. This expression holds only for films of densities above the percolation threshold and with a uniform distribution of nanotube end-sites. For a more detailed derivation from single-SWCNT behavior, including broader case analysis, see ref 10.

At steady state the exciton transport expression (eq 2) is therefore described by a nonlinear, nonhomogenous ordinary differential equation (ODE) of simplified form,[10]

$$D_z\frac{d^2c}{dz^2} - k_1 c - k_2 c^2 = -N(z) \quad (3)$$

Note that all parameters are extracted from individual/aggregate SWCNT photophysics and the distribution of nanotube orientations in the film. The ODE is subject to Robin boundary conditions describing Type II exciton dissociation at each interface, $z = 0,T$ for a film of thickness $T$,

$$\pm D_z\frac{dc}{dz}\bigg|_{z=0,T} = k_d c|_{z=0,T} \quad (4)$$

where $k_d$, the dissociation rate constant, we take to infinity in the rapid-dissociation limit, checking that the flux converges.

*Analytic Solution to Photoadsorption of the Solar Spectrum in SWCNT Films.* The first obstacle to analytic evaluation of (3) is $N(z)$, the exciton generation rate, which is the photon absorption rate. A valid form of $N(z)$ that enables facile solution to the exciton transport ODE is the usual inhibitor to analytic or even deterministic solutions to exciton-transport-limited nanomaterial photovoltaic models. Herein we report an analytic expression with material-specific physical constants that captures that light absorption behavior.

$N(z)$ is the product of the absorption cross-section per nanotube $\sigma_l(\boldsymbol{\epsilon}, \hat{\mathbf{l}}, \omega)$, the number density $\rho_{\langle l \rangle}$, and the solar flux at depth $z$ $J_\nu(\omega, \epsilon|z)$,

$$N(\omega, \boldsymbol{\epsilon}|z) = \rho_{\langle l \rangle}\cdot\sigma_l(\boldsymbol{\epsilon}, \hat{l}, \omega)\cdot J_\nu(\omega, \boldsymbol{\epsilon}|z) \quad (5)$$

$N(\omega, \boldsymbol{\epsilon}|z)$ carries a frequency $\omega$ and polarization $\boldsymbol{\epsilon}$ dependence, the latter of which demands a SWCNT orientation $\hat{\mathbf{l}}$ dependence. $N(z)$ is then a quadruple integral over the nanotube orientation distribution $p(\theta, \phi)$, linear in-plane polarization $\boldsymbol{\epsilon}$ (we assume normally incident light), and light frequency $\omega$,

$$N(z) = \rho_{\langle l \rangle}\int_0^\infty\int_0^{2\pi} J_\nu(\omega, \epsilon|z) \times \int_0^{2\pi}\int_0^{\pi}\sigma_l(\epsilon, [\theta, \phi], \omega)p(\theta, \phi)\, d\theta\, d\phi\, d\epsilon\, d\omega \quad (6)$$

where $\rho_{\langle l \rangle}$ is the nanotube density (length of nanotube per volume of film), $J_\nu$ is the photon flux, and $\sigma_l$ is the single-SWCNT absorption cross-section, per length of nanotube.

To proceed, we focus on devices with isotropic in-plane light absorption and no reflection of light off the back electrode. This parametric space is the most relevant to technological interests; in the former case it includes isotropic and vertically aligned films, which we previously showed present dominant efficiency relative to films with anisotropic in-plane alignment. In the latter case, a transparent back electrode takes advantage of SWCNTs near-infrared (nIR) absorption by allowing the solar cell to complement existing visible PVs or coat building materials. Those approximations make the polarization and nanotube orientation integrals trivial. We then solve the differential equation describing the light field attenuation as it passes through the film,

$$\frac{dJ_\nu(\omega|z)}{dz} = -N(\omega|z) \Rightarrow J_\nu(\omega|z) = J_0(\omega)\cdot\exp[-\rho_{\langle l \rangle}\cdot\sigma_l(\omega)\cdot z] \quad (7)$$

where $J_0(\omega)$ is the incident solar flux. That produces the final integral over frequency space

$$N(z) = \rho_{\langle l \rangle}\int_0^\infty J_0(\omega)\sigma_l(\omega)\exp[-\rho_{\langle l \rangle}\cdot\sigma_l(\omega)\cdot z]\, d\omega \quad (8)$$



DOI: 10.1021/acs.jpclett.6b01053
J. Phys. Chem. Lett. 2016, 7, 2683−2688

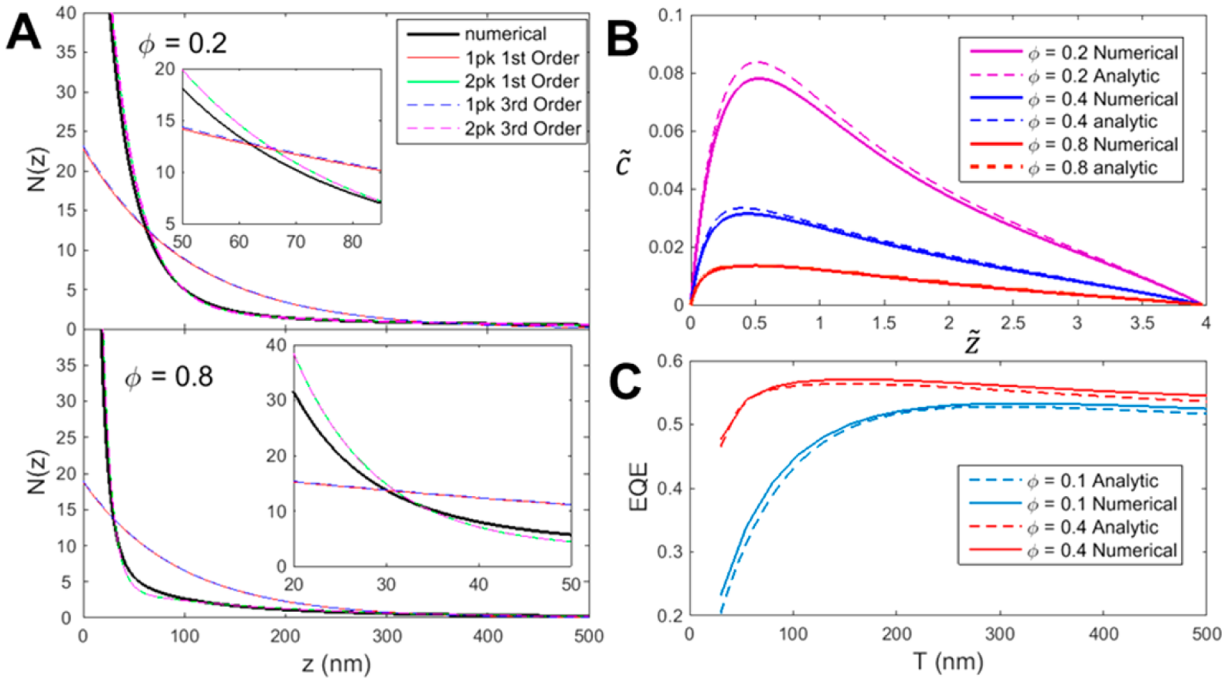


**Figure 2.** Comparison of analytic and numerical solutions. (A) Solution to the photon absorption rate, comparing the numerical result (black) to the analytic solutions with one or two absorption peaks and first- or third-order Gaussian-exponential Taylor expansion. Solutions for 20% and 80% close-packed density are shown, with insets zoomed for clarity. While it is necessary to include absorption from both SWCNT electronic transitions, we can see that a third-order Taylor expansion of the frequency integrand is unnecessary. (B) Nondimensional exciton concentration profiles comparing the numerical and analytic solutions at different densities for a film of thickness $\tilde{z} = 4$. (C) Film EQE as a function of film thickness at different densities.

To solve that integral, we recognize several simplifications. First we can very closely approximate the nanotube absorption spectrum as a series of Gaussian functions for each absorption peak, with magnitude $S_a$,

$$\sigma_l(\omega) = \sum_a S_a \cdot \exp\left[-\frac{(\omega - \mu_a)^2}{2\sigma_a^2}\right] \tag{9}$$

where $\mu_a$ is the energy of the transition, and $\sigma_a$ is the peak width (FWHM $= 2\sqrt{2\ln 2}\,\sigma_a$). Next, we find that because the SWCNT absorption peaks lie on only the red side of the solar spectrum peak, the spectrum can be sufficiently approximated as a Gaussian as well,

$$J_0(\omega) \cong J_0 \cdot \exp\left[-\frac{(\omega - \mu_J)^2}{2\sigma_J^2}\right] \tag{10}$$

Those simplifications make $N(z)$ an insoluble convolution of a Gaussian and an exponential decay of a Gaussian (see SI). We can observe, however, that while the Exponential-Gaussian term is in general not well captured by the first-order Taylor expansion, its product with the Gaussian term *is* because either the function extrema are close *or* the Gaussian-Exponential reduces to unity. That observation simplifies the integral, allowing us to solve it as

$$N(z) = \rho_{\langle l\rangle} J_0 \sum_{a=1}^{2} S_a \gamma_a \sqrt{2\pi} \cdot e^{-\rho_{\langle l\rangle} S_a z} \tag{11}$$

where $\gamma_a$ can be understood as the area of overlap of the solar flux and absorption peak $a$,

$$\gamma_a \equiv \sigma_{Ja} e^{-(\mu_J - \mu_a)^2/2(\sigma_J^2 + \sigma_a^2)},\ \sigma_{Ja} \equiv \sqrt{\frac{\sigma_J^2 \sigma_a^2}{\sigma_J^2 + \sigma_a^2}} \tag{12}$$

The sum must include two peaks for each SWCNT chirality, corresponding to the $E_{1u}$ and $E_{2u}$ transitions. For a solid film of (6,5) SWCNT,[7] the empirical constants are $S_1 = 1.64 \times 10^{-10}$ m$^2$/m, $\gamma_1 = 293$ nm, $S_2 = 0.13 \times 10^{-10}$ m$^2$/m, and $\gamma_2 = 74$ nm.

This biexponential analytic expression closely matches the numerical solution (Figure 2A). The curve can be understood as light absorption on two length-scales, one for each portion of the frequency spectrum absorbed. Because there are two absorption peaks with different absorption cross sections, near-IR absorption being stronger, light at nIR frequencies is, relative to initial intensity, attenuated rapidly while visible light is absorbed more gradually, providing a long tail to our generation rate. That effect is emphasized by the greater incident solar intensity at the visible vs nIR frequencies. We can also see evidenced that our first-order Taylor expansion of the Gaussian-exponential is sufficient, with essentially no benefit to a third-order expansion.

*Analytical Solution to the Exciton Transport Model.* With an analytic expression for $N(z)$ we are able to nondimensionalize the ODE (eq 3). The problem symmetry yields the characteristic exciton concentration and Cartesian length,

$$c_0 \equiv \frac{J_0 \cdot \rho_{\langle l\rangle} S_1 \cdot \gamma_1}{k_1 n_1} \tag{13}$$

$$z_0 \equiv \sqrt{\frac{D_z}{k_1 n_1}} = L_D \tag{14}$$



DOI: 10.1021/acs.jpclett.6b01053
J. Phys. Chem. Lett. 2016, 7, 2683−2688

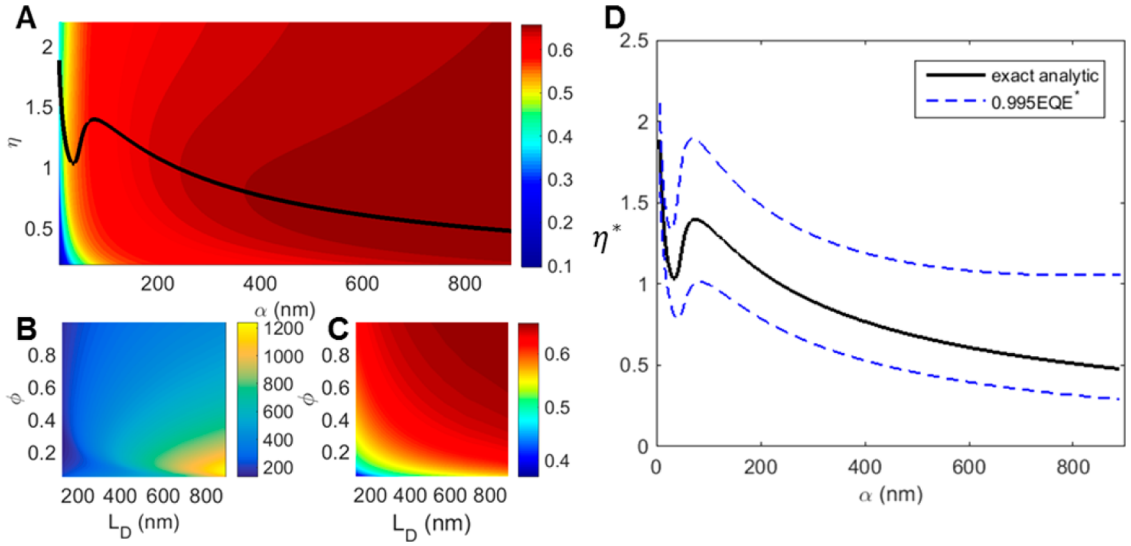


**Figure 3.** (A) Photovoltaic external quantum efficiency (EQE) as a function of film thickness $\eta$ and parameter grouping $\alpha$. Note that a nonlinear color bar was used for visual clarity. At a given $\alpha$ there is an optimal thickness $\eta^*$ that maximizes the EQE, indicated by the black line overlay. (B) the EQE-maximizing thickness $T^* = \eta^* L_D$ versus density $\phi$ and exciton diffusion length $L_D$. (C) Maximum achievable EQE versus density $\phi$ and exciton diffusion length $L_D$, showing the monotonic increase in both. In both panels B and C, $\alpha$ is the product of the axes. (D) Master curve (black) of optimal device thickness, nondimensionalized with the exciton diffusion length $\eta^* \equiv T^*/L_D$, versus $\alpha$, the product of diffusion length and normalized density and the sole system parameter. Measuring a SWCNT film's $\alpha$ dictates the optimal device thickness for that material. Blue dashed curves indicate the bounds of higher and lower thickness that yield an EQE above 99.5% of the maximum. The broad EQE tolerance suggests that in lieu of measuring $\alpha$, choosing $\eta$ between 0.6 and 1.4, i.e., $T^* \cong L_D$ will provide essentially optimal performance.

where peak 1 (implied in $S_1$, $\gamma_1$) is the dominant absorption mode, and $k_1 n_1$ is the product of the single-nanotube first-order quenching rate constant and the concentration of impurities including nanotube ends. Multiple impurities with different rate constants can be treated with a weighted sum. The characteristic variables $c_0$ and $z_0$ reflect the physical trade-offs of the system. The nondimensional concentration is a ratio of the exciton generation rate to the dominant exciton quenching rate, which compete to increase and decrease, respectively, the exciton concentration. The nondimensional Cartesian coordinate normalizes the film thickness as $\eta \equiv T/L_D$, which balances the film thickness against the effective exciton diffusion length in the film. A thicker film or lower diffusion length reduces the number of excitons that reach the electrodes.

Substituting nondimensional concentration $\tilde{c} \equiv c/c_0$ and Cartesian dimension $\tilde{z} \equiv z/z_0$ into the exciton balance, we are left with

$$\frac{d^2\tilde{c}}{d\tilde{z}^2} - \left(\frac{k_\Gamma}{k_1 n_1} + 1\right)\tilde{c} - \frac{k_2(\rho_{\langle l\rangle} J_0 S_1 \gamma_{11})}{(k_1 n_1)^2}\tilde{c}^2 = -\sqrt{2\pi}\sum_{a=1}^{2}\frac{S_a\gamma_a}{S_1\gamma_1}\cdot e^{-\rho_{\langle l\rangle}S_a\sqrt{D_z/k_1 n_1}\tilde{z}} = -\sqrt{2\pi}\left(e^{-\rho_{\langle l\rangle}S_1 L_D\tilde{z}} + \frac{S_2\gamma_2}{S_1\gamma_1}\cdot e^{-\rho_{\langle l\rangle}S_2 L_D\tilde{z}}\right) \quad (15)$$

We then compare the magnitude of terms, finding that those much less than unity are negligible to yield the far simplified exciton balance

$$\frac{d^2\tilde{c}}{d\tilde{z}^2} - \tilde{c} = -\sqrt{2\pi}\left(e^{-\tau_1\alpha\tilde{z}} + \frac{S_2\gamma_2}{S_1\gamma_1}\cdot e^{-\tau_2\alpha\tilde{z}}\right) \quad (16)$$

$$\left.\frac{d\tilde{c}}{d\tilde{z}}\right|_{\tilde{z}=0} = \kappa\tilde{c}(0), \qquad \left.\frac{d\tilde{c}}{d\tilde{z}}\right|_{\tilde{z}=\eta} = -\kappa\tilde{c}(\eta) \quad (17)$$

$$\alpha \equiv \phi\cdot L_D, \quad \phi \equiv \frac{\rho_{\langle l\rangle}}{\rho_{\langle l\rangle}^{CP}}, \quad \eta \equiv \frac{T}{L_D}, \quad \kappa \equiv \frac{k_d}{\sqrt{D_z k_1 n_1}}, \quad \tau_a \equiv S_a\rho_{\langle l\rangle}^{CP} \quad (18)$$

Solving with the method of undetermined coefficients and taking the rapid-dissociation limit, we find the concentration profile is a balance of four competing exponentials,

$$\tilde{c}(\tilde{z}) = \beta_1 e^{\tilde{z}} + \beta_2 e^{-\tilde{z}} - \frac{1}{(\tau_1\alpha)^2 - 1}e^{-\tau_1\alpha\tilde{z}} - \sqrt{2\pi}\frac{S_2\gamma_2}{S_1\gamma_1}\frac{1}{(\tau_2\alpha)^2 - 1}e^{-\tau_2\alpha\tilde{z}} \quad (19)$$

$$\beta_1 = -\frac{1}{e^{\eta} - e^{-\eta}}\left(\frac{e^{-\eta} - e^{-\tau_1\alpha\eta}}{(\tau_1\alpha)^2 - 1} + \sqrt{2\pi}\frac{S_2\gamma_2}{S_1\gamma_1}\frac{e^{-\eta} - e^{-\tau_2\alpha\eta}}{(\tau_2\alpha)^2 - 1}\right) \quad (20)$$

$$\beta_2 = +\frac{1}{e^{\eta} - e^{-\eta}}\left(\frac{e^{\eta} - e^{-\tau_1\alpha\eta}}{(\tau_1\alpha)^2 - 1} + \sqrt{2\pi}\frac{S_2\gamma_2}{S_1\gamma_1}\frac{e^{\eta} - e^{-\tau_2\alpha\eta}}{(\tau_2\alpha)^2 - 1}\right) \quad (21)$$

The result we again check against the numerical solution (Figure 2B), finding excellent agreement to validate our approximations. Our biexponential light field decay due to a weak and strong absorption peak manifests in a pronounced tail in exciton concentration toward the back electrode; nIR light (the stronger peak, $\tau_1$) is rapidly collected, while visible light (the weaker peak, $\tau_2$) is more weakly absorbed to generate excitons deeper in the film.



DOI: 10.1021/acs.jpclett.6b01053
J. Phys. Chem. Lett. 2016, 7, 2683−2688

In the exciton-transport-limited approximation, we can estimate the EQE from the boundary solutions

$$\mathrm{EQE}(\eta) \propto D_z\left(\left.\frac{dc}{dz}\right|_{z=0} - \left.\frac{dc}{dz}\right|_{z=T}\right) = J_0\gamma_1\tau_1 \alpha\left(\left.\frac{d\tilde{c}}{d\tilde{z}}\right|_{\tilde{z}=0} - \left.\frac{d\tilde{c}}{d\tilde{z}}\right|_{\tilde{z}=\eta}\right) \quad (22)$$

We can optimize eq 22, setting its derivative equal to zero to find the maximum as (Figure 2C),

$$\begin{aligned}\frac{d\mathrm{EQE}}{d\eta} &= 0 \\ &= F_1((1-p_1)e^{-\eta^*(\tau_1\alpha)} + (2p_1)e^{-\eta^*(\tau_1\alpha-1)} \\ &\quad + (2m_1p_1 - 2)e^{-\eta^*(\tau_1\alpha-2)} + (-2m_1)e^{-\eta^*(\tau_1\alpha-3)} \\ &\quad + (1+m_1)e^{-\eta^*(\tau_1\alpha-4)}) + F_2((1-p_2)e^{-\eta^*(\tau_2\alpha)} \\ &\quad + (2p_2)e^{-\eta^*(\tau_2\alpha-1)} + (2m_2p_2 - 2)e^{-\eta^*(\tau_2\alpha-2)} \\ &\quad + (-2m_2)e^{-\eta^*(\tau_2\alpha-3)} + (1+m_2)e^{-\eta^*(\tau_2\alpha-4)}) \\ &\quad + (2m_1p_1F_1 + 2m_2p_2F_2)(2e^{2\eta^*} - e^{\eta^*} - e^{3\eta^*})\end{aligned} \quad (23)$$

$$m_a \equiv \frac{1}{\tau_a\alpha - 1}, \quad p_a \equiv \frac{1}{\tau_a\alpha + 1}, \quad F_a \equiv \sqrt{2\pi}\frac{S_a\gamma_a}{S_1\gamma_1} \quad (24)$$

Crucially, there is only one film parameter in this expression, $\alpha$, the product of film density and the effective exciton diffusion length in the film. The optimal thickness therefore depends on only this single variable, and all possible films collapse to a single $\eta$–$\alpha$ space, as in Figure 3A.

*Discussion*. Examining the efficiency variation with thickness and $\alpha$ (Figure 3A), we can observe that EQE monotonically increases with $\alpha$; higher $\alpha$ materials, which have higher densities and exciton diffusion lengths, are unambiguously better (Figure 3C). In particular, there is a sharp drop in efficiency for $\alpha$ below 10 nm, indicating that a mean exciton diffusion length of over 100 nm for a 10% close-packed film or 10 nm for a 100% close-packed film is a crucial material property that must be achieved to advance SWCNT Solar Cell technology. Additionally, at a given $\alpha$ there is an optimal $\eta^*$, indicated by the black line in Figure 3A. The optimum represents a balance between a thicker film collecting more light but increasing the distance that excitons must travel to reach the electrodes. At higher densities ($\phi$) more light is collected per unit thickness, increasing the maximum EQE and reducing the optimal thickness required to achieve it. At longer diffusion lengths ($L_D$) excitons are collected more efficiently, allowing the film to be thicker to achieve the same efficiency or to increase the EQE at the same thickness. These cooperative effects are captured in the product $\alpha$, with the only difference being that $L_D$'s thickness-increasing attribute is balanced by $\eta$'s normalization to $L_D$, which is clear in Figure 3B; as $L_D$ increases and the density decreases, the optimal thickness rises. From this examination we can finally address the practically achievable morphology trade-off between increasing density and increasing diffusion length, such as encountered when choosing between isotropic and vertically aligned films using current techniques: because the product of $\phi$ and $L_D$ is the driver of EQE, they should match. This is demonstrated in the symmetry of Figure 3C. Roughly, EQE is maximal when $\phi$ is about 1/1000th of $L_D$ in nm.

In hindsight the reduction of the system to $\alpha$ is intuitive: the rate of light absorption (exciton generation) is dictated by the film density, while the rate of exciton collection is dictated by the diffusion length (and film thickness). Higher density and higher $L_D$ increase the rate of charge collection cooperatively. Having reduced the system to this single parameter, we can construct the master curve Figure 3D. To employ this curve, an experimentalist only needs to measure her SWCNT film's $\alpha$, ideally having increased it as much as possible (Figure 3C). Above very low $\alpha$ (10 nm), The EQE has a plateau-like cross-section (Figure 2C) that makes it drop off suddenly far from $\eta^*$, but fairly invariant close to $\eta^*$. As a result, there is a high degree of EQE-tolerance in the region around $\eta^*$, exemplified by the blue bounds in Figure 3D within which the EQE is ≥99.5% of the maximum possible EQE. That tolerance means that even if experimenters do not measure their $\alpha$, they can comfortably approximate $0.6 \leq \eta^* \leq 1.4$ or, equivalently, $T^* \cong L_D$. In other words, near-maximal performance can be achieved by setting the device thickness equal to the exciton diffusion length in the charge-collecting axis.

Under the simplifications we have made, that result has quite broad applicability to any excitonic photovoltaic material with bell-shaped absorption modes. The rule of thumb breaks down at two extremes: very high and very low $\alpha$. The latter case is physically realistic; it is sparse films, or materials with very low optical absorptivity. In those cases, the optimal thickness becomes many times the diffusion length due to the poor light collection. The other limit of very high $\alpha$ can be imagined as extremely high light absorption, where the exciton diffusivity becomes irrelevant and the film should be as thin as possible, i.e., $\eta^* \ll 1$, $T^* \ll L_D$. This case is not physically realistic with existent materials however; SWCNT already have very high optical absorptivity compared to most photovoltaic materials, and density is constrained to a maximum of close-packed density. As a result, our maximum $\alpha$ considered in Figure 3D is unlikely to be exceeded by any other material.

In summary, we find that the characteristic spatial length scale describing SWCNT PVs is the exciton diffusion length, $L_D = \sqrt{D_z/k_1n_1}$, where $D_z$ is the exciton diffusivity in the charge-collecting axis and $k_1n_1$ is the first-order quenching rate constant, i.e., the balance of exciton reaction and diffusion. Nondimensionalizing device thickness as $\eta \equiv T/L_D$, the efficiency-maximizing thickness $\eta^*$ depends on a *single* grouping of parameters, $\alpha = \phi \cdot L_D$, where $\phi$ is the SWCNT number density normalized to close-packed. That generates a master $\eta^*(\alpha)$ curve (Figure 3D) that any device can be placed on, empowering device-makers to know their optimal thickness simply by measuring their material's $\alpha$. We further find that close to the optimum, external quantum efficiency (EQE) is only weakly variant with $\eta$, yielding the rule of thumb $0.6 \leq \eta^* \leq 1.4$, or equivalently $T^* \cong L_D$, the thickness equals the diffusion length, which provides an EQE within 0.5% of the maximum. Finally, our solution is enabled by a new method of approximating absorption of the solar flux that is applicable to any film with bell-shaped, isotropic absorption peaks. The light absorption (carrier generation) gradient is generally the most difficult component of photovoltaic performance to solve due to the convolution of nonlinear incident intensity and absorption spectrum over frequency and polarization. Our treatment as a whole applies to any exciton-transport-limited



DOI: 10.1021/acs.jpclett.6b01053
J. Phys. Chem. Lett. 2016, 7, 2683−2688

film with those absorption properties, with an analytic vs numerical error less than 1% of the resulting EQE.

## ■ ASSOCIATED CONTENT

### Supporting Information

The Supporting Information is available free of charge on the ACS Publications website at DOI: 10.1021/acs.jpclett.6b01053.

Step-by-step derivation of our solution, as well as additional figures examining model results (PDF)

## ■ AUTHOR INFORMATION

### Corresponding Author

*E-mail: strano@mit.edu.

### Notes

The authors declare no competing financial interest.

## ■ ACKNOWLEDGMENTS

M.S.S. acknowledges a grant from Eni S.p.A. in the frame of the eni-MIT Solar Frontiers Center. D.O.B. thanks the United States Department of Defense for the National Defense Science and Engineering Graduate Fellowship.

## ■ REFERENCES

(1) Chen, X.; Li, C.; Gratzel, M.; Kostecki, R.; Mao, S. S. *Chem. Soc. Rev.* **2012**, *41*, 7909.
(2) Jariwala, D.; Sangwan, V. K.; Lauhon, L. J.; Marks, T. J.; Hersam, M. C. *Chem. Soc. Rev.* **2013**, *42*, 2824.
(3) Kanai, Y.; Wu, Z.; Grossman, J. C. *J. Mater. Chem.* **2010**, *20*, 1053.
(4) Nelson, J.; Kwiatkowski, J. J.; Kirkpatrick, J.; Frost, J. M. *Acc. Chem. Res.* **2009**, *42*, 1768.
(5) Labat, F.; Le Bahers, T.; Ciofini, I.; Adamo, C. *Acc. Chem. Res.* **2012**, *45*, 1268.
(6) Shluger, A. L.; McKenna, K. P.; Sushko, P. V.; Ramo, D. M.; Kimmel, A. V. *Modell. Simul. Mater. Sci. Eng.* **2009**, *17*, 084004.
(7) Jain, R. M.; Howden, R.; Tvrdy, K.; Shimizu, S.; Hilmer, A. J.; McNicholas, T. P.; Gleason, K. K.; Strano, M. S. *Adv. Mater.* **2012**, *24*, 4436.
(8) Shea, M. J.; Arnold, M. S. *Appl. Phys. Lett.* **2013**, *102*, 243101.
(9) Ren, S. Q.; Bernardi, M.; Lunt, R. R.; Bulovic, V.; Grossman, J. C.; Gradecak, S. *Nano Lett.* **2011**, *11*, 5316.
(10) Bellisario, D. O.; Jain, R. M.; Ulissi, Z.; Strano, M. S. *Energy Environ. Sci.* **2014**, *7*, 3769.



DOI: 10.1021/acs.jpclett.6b01053
*J. Phys. Chem. Lett.* 2016, 7, 2683−2688